Electronic Supplementary Information for

Mo-doped Ni_2P Hollow Nanostructures: Highly Efficient and Durable Bifunctional Electrocatalysts for Alkaline Water Splitting

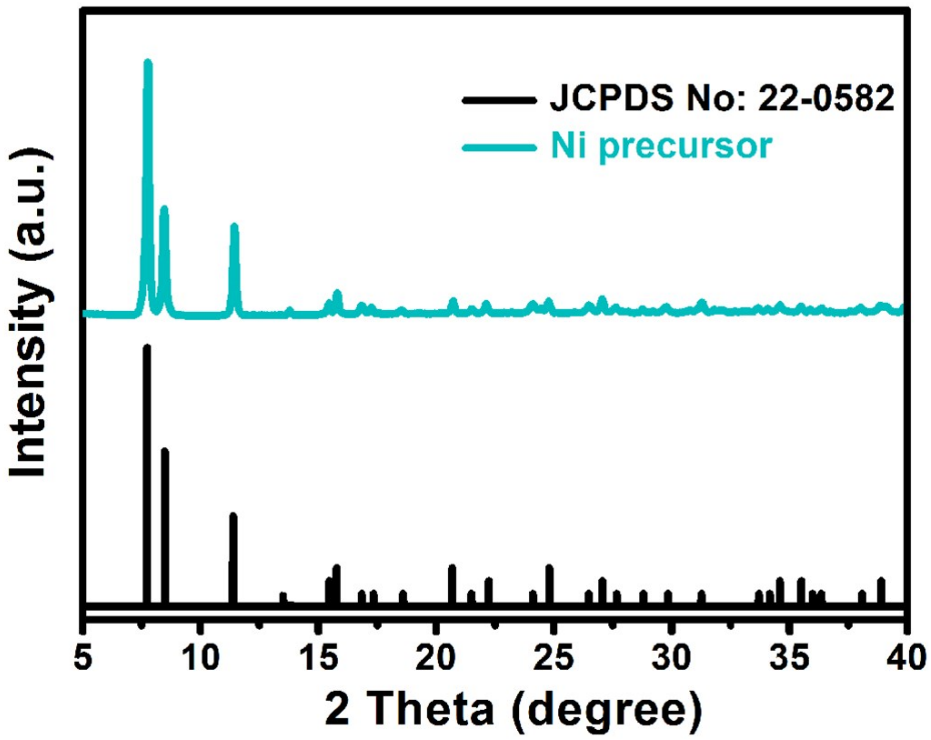

Fig. S1 XRD pattern of Ni nanoprism precursor.

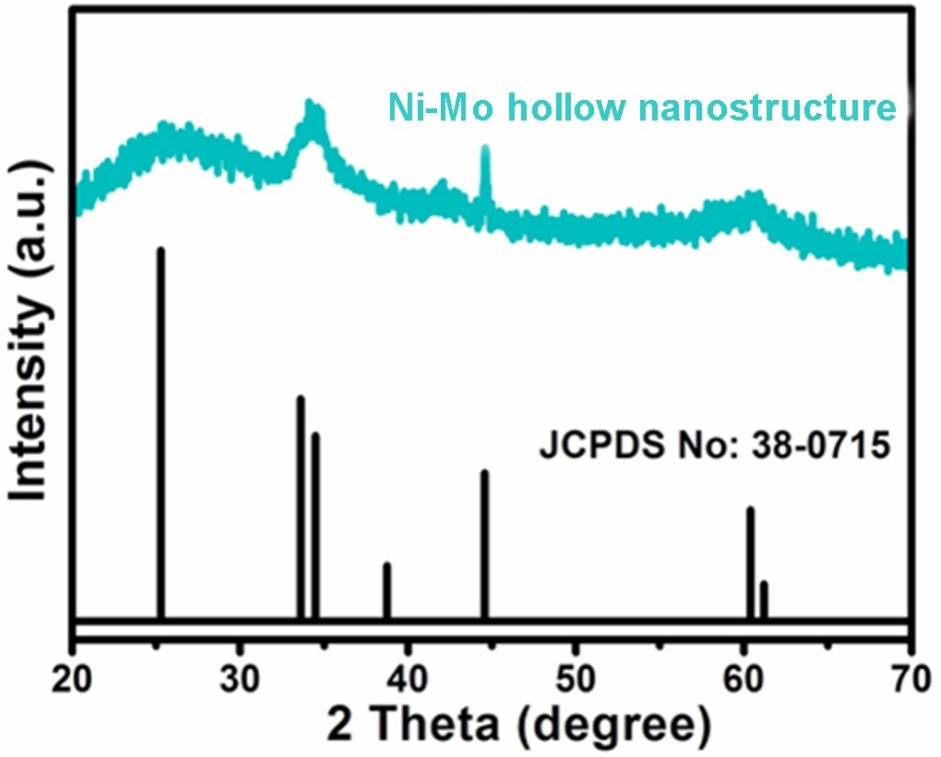

Fig. S2 XRD pattern of Ni-Mo hollow nanostructure.

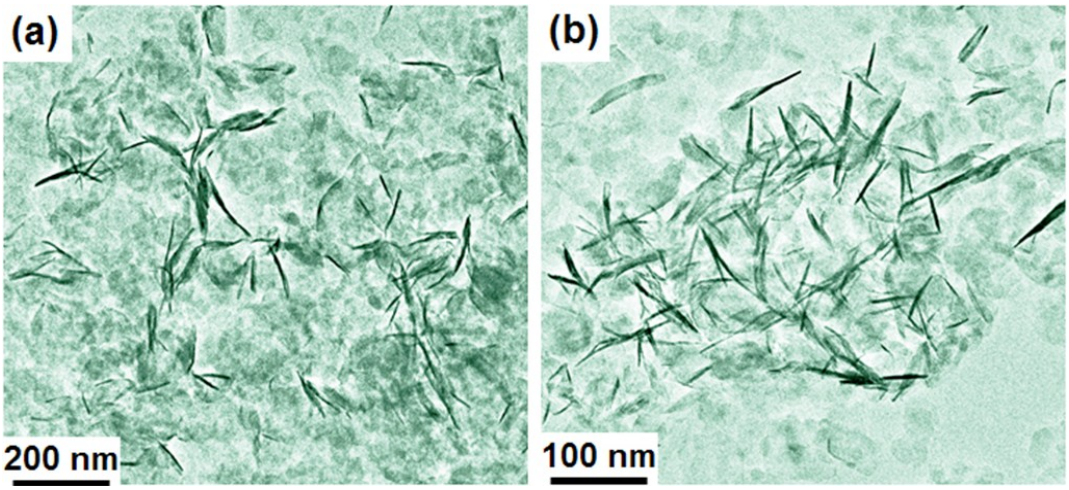

Fig. S3 (a-b) TEM images of the Ni-Mo nanosheets without using the 0.2 M HCl solution as pH regulator after 12 h solvothermal reaction.

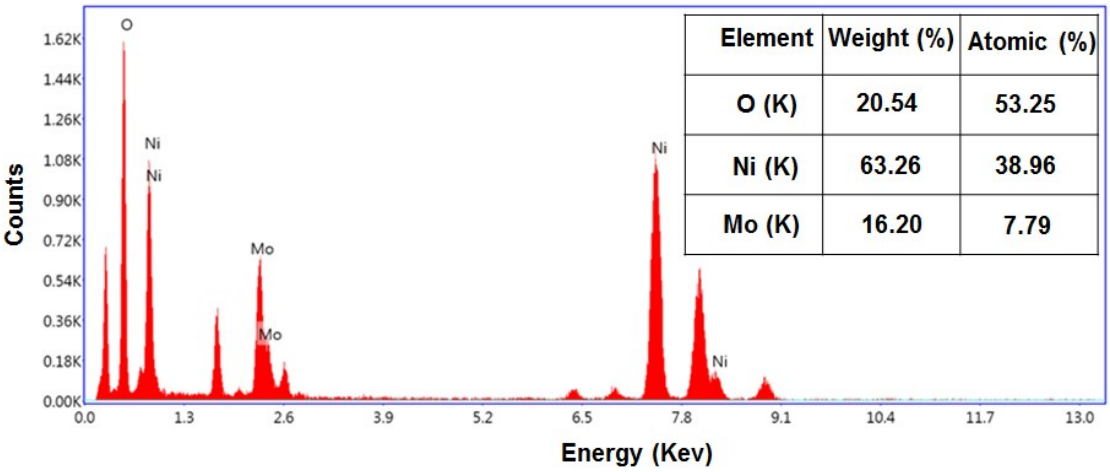

Element	Weight (%)	Atomic (%)
O (K)	20.54	53.25
Ni (K)	63.26	38.96
Mo (K)	16.20	7.79

Fig. S4 TEM-EDS spectrum of the Ni-Mo hollow nanostructure.

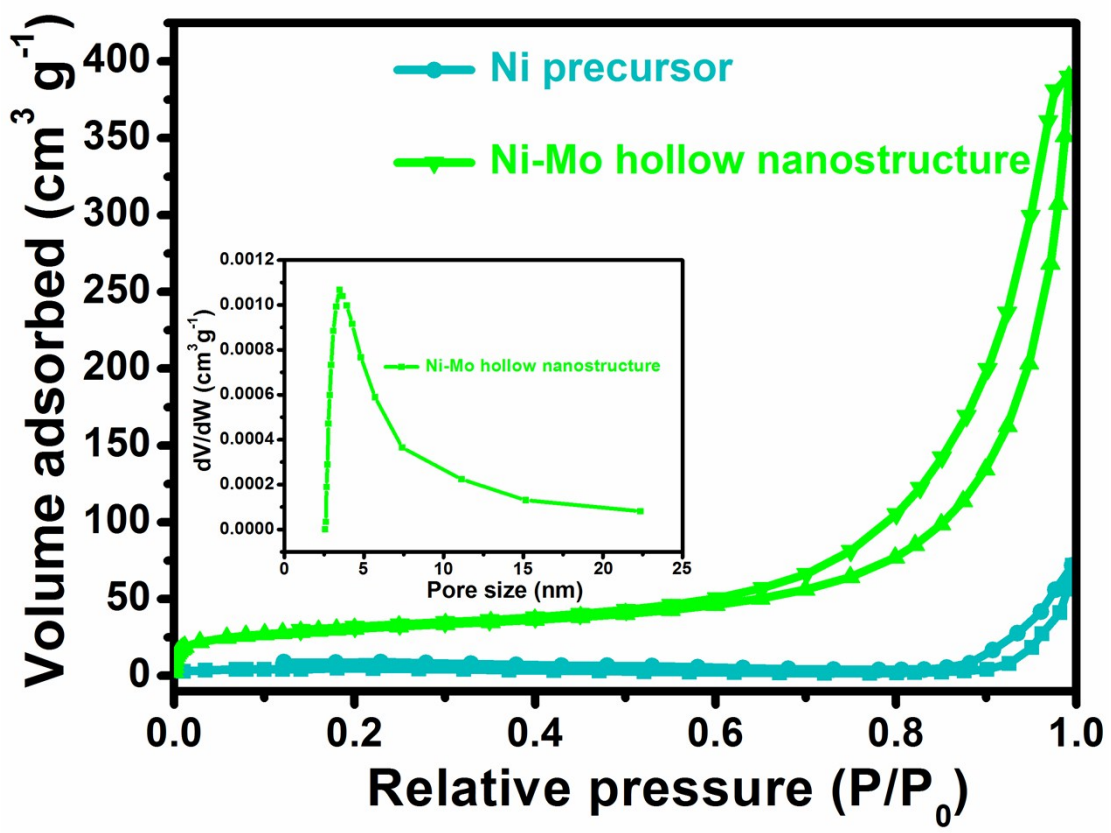

Fig. S5 N_2 adsorption/desorption isotherms of Ni nanoprism precursor and Ni-Mo hollow nanoprism. Inset: pore size distribution of Ni-Mo hollow nanostructure.

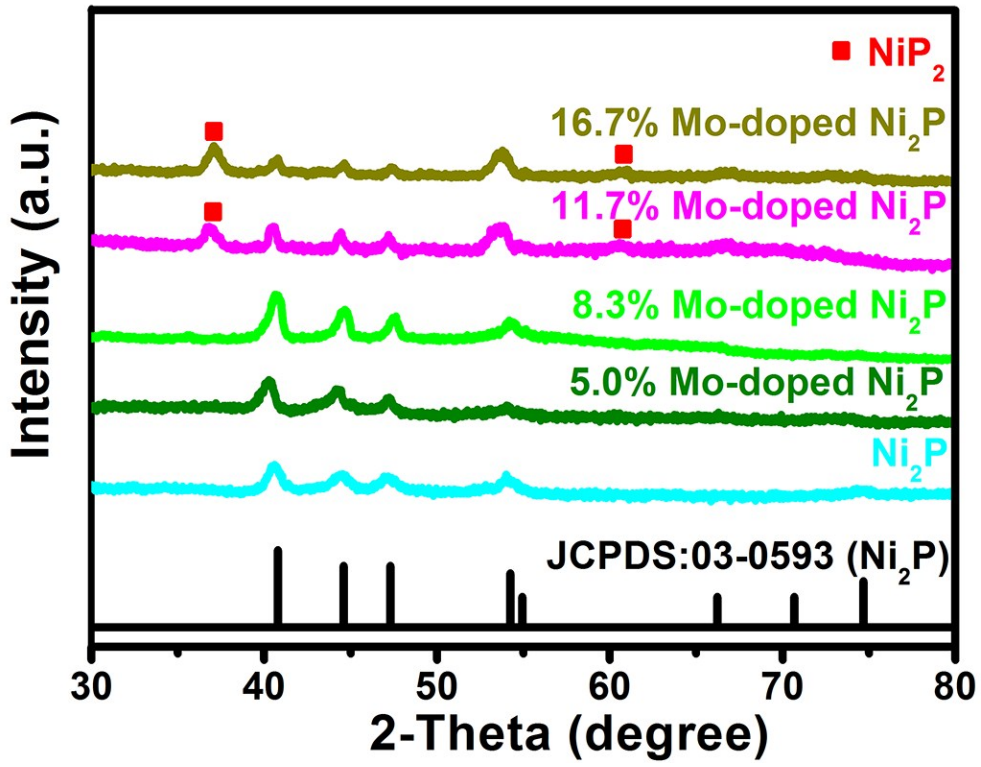

Fig. S6 XRD patterns of pristine Ni_2P and different mass ratios of Mo-doped Ni_2P hollow nanostructure.

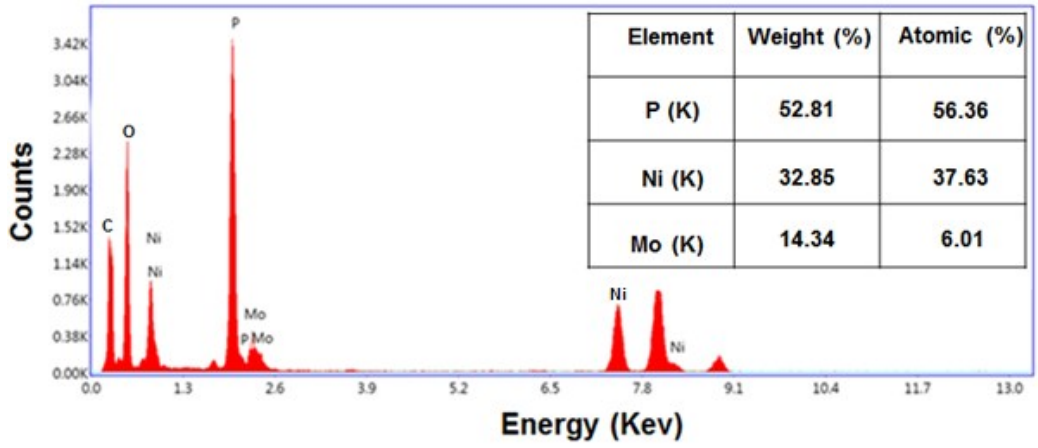

Fig. S7 TEM-EDS spectrum of the Mo-doped Ni_2P hollow nanostructure.

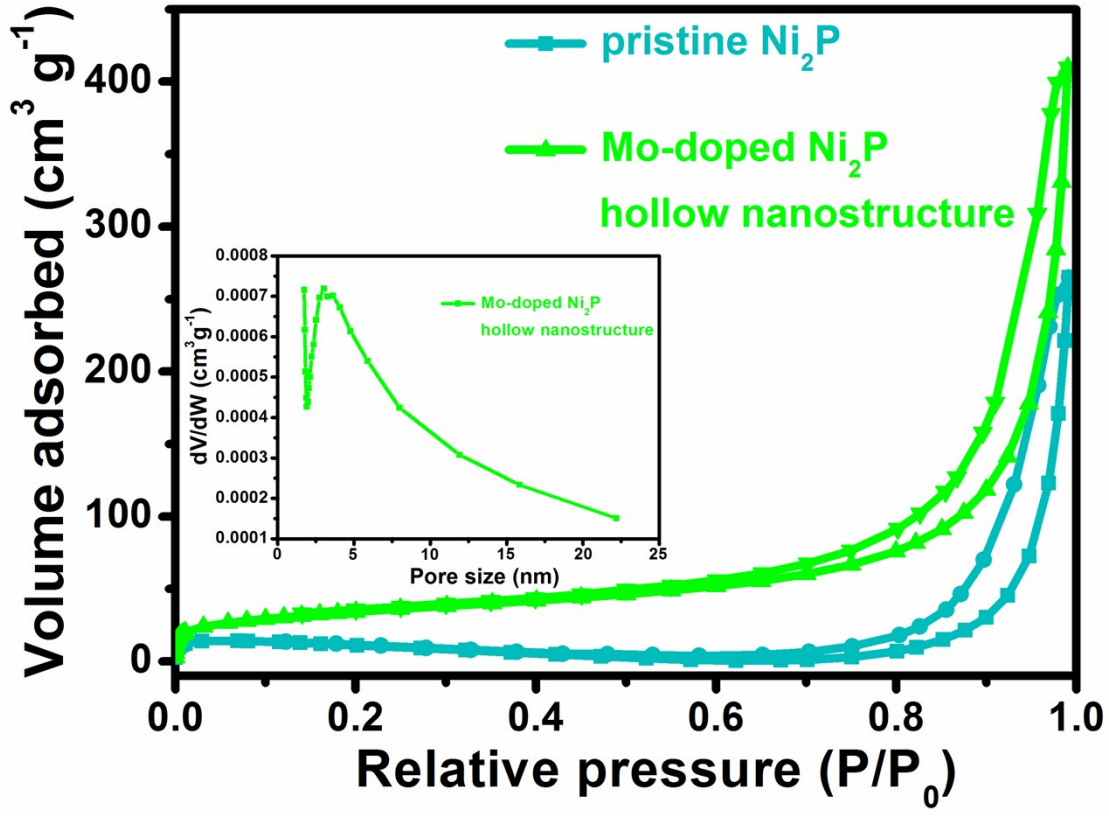

Fig. S8 N_2 adsorption/desorption isotherms of pristine Ni_2P and Mo-doped Ni_2P hollow nanostructures. Inset: pore size distribution of Mo-doped Ni_2P hollow nanostructures.

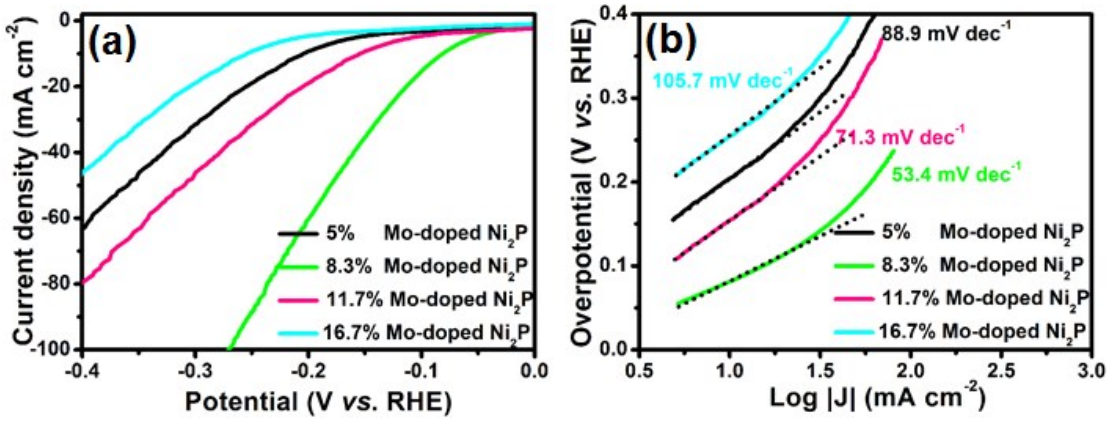

Fig. S9 (a) Polarization curves and (b) Corresponding Tafel plots of the series of the different mass ratio of Mo-doped Ni_2P hollow nanostructures.

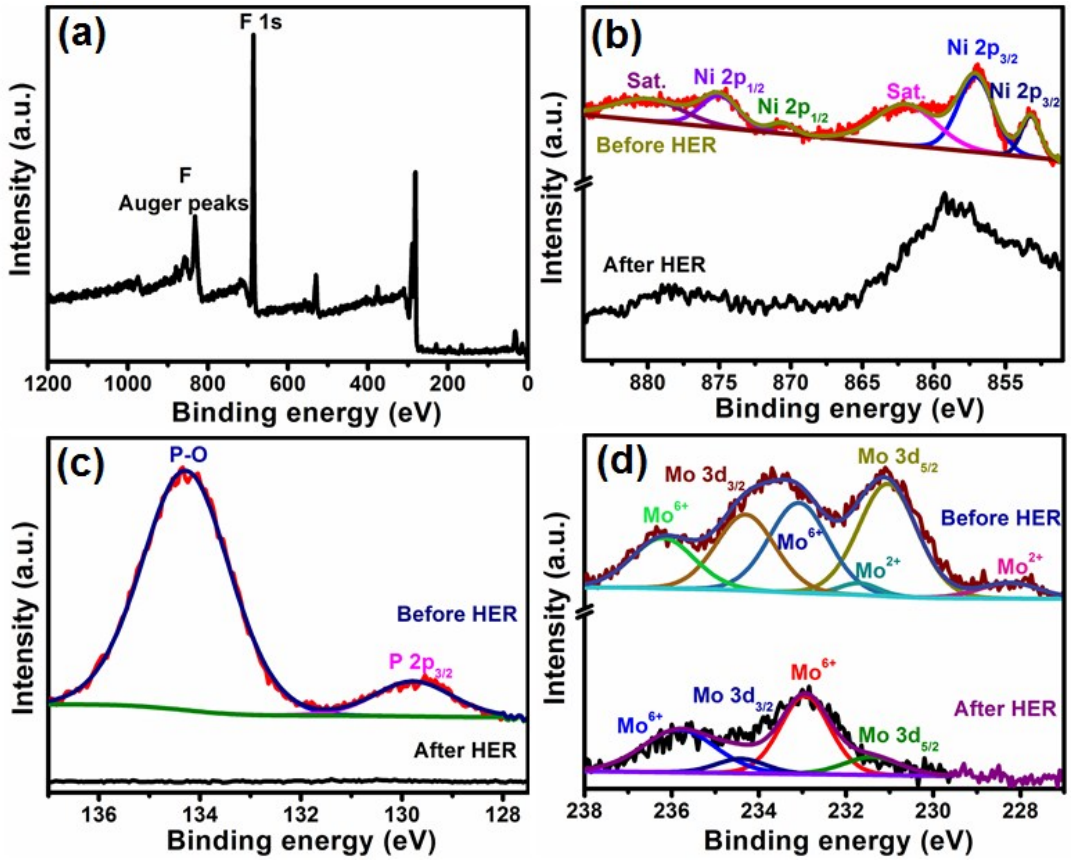

Fig. S10 Survey scan (a) and high-resolution XPS spectra of the Mo-doped Ni_2P hollow nanostructures: (b) Ni 2p, (c) P 2p and (d) Mo 3d after 10 HER stability test.

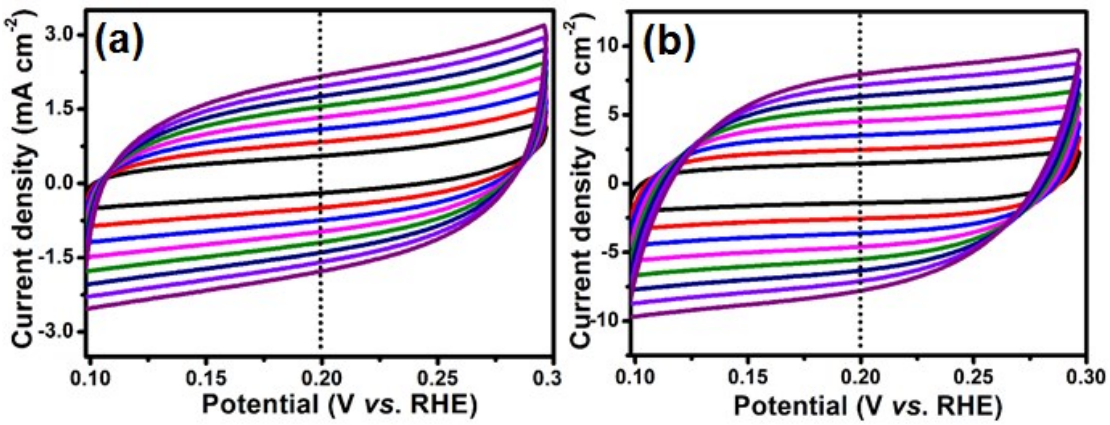

Fig. S11 Voltammograms of the (a) pristine Ni_2P and (b) Mo-doped Ni_2P hollow nanostructures at various scan rates (20-160 mV s^{-1}) during the HER process in alkaline electrolyte.

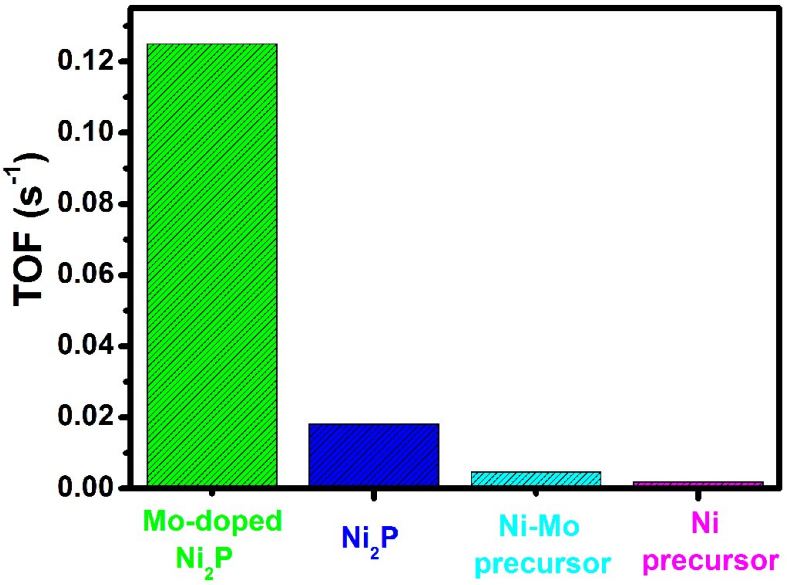

Fig. S12 TOFs of the Mo-doped Ni_2P hollow nanostructures, pristine Ni_2P, Ni-Mo precursor and Ni precursor during the HER process.

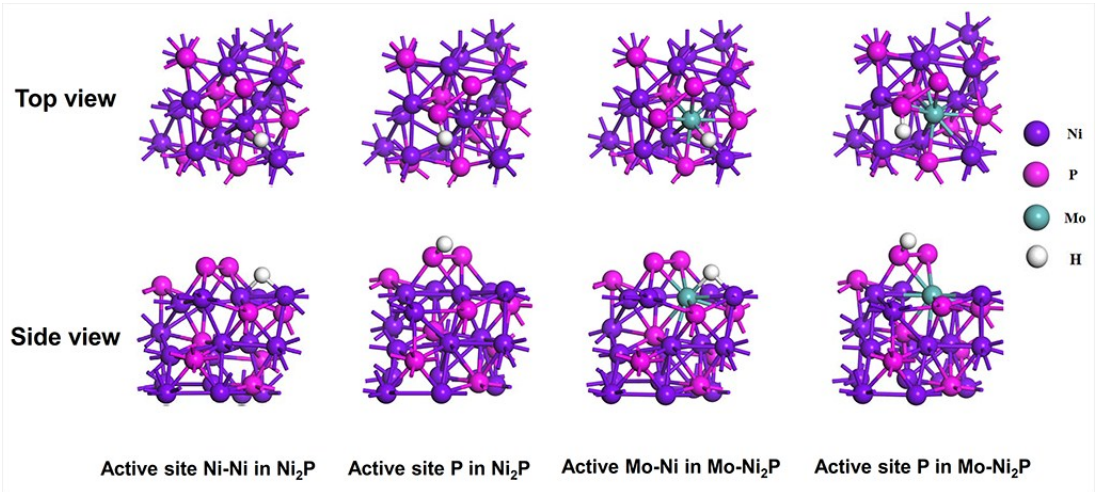

Fig. S13 Top and side views of the pristine Ni_2P (111) and Mo-doped Ni_2P (111) with four types

of relatively stable sites.

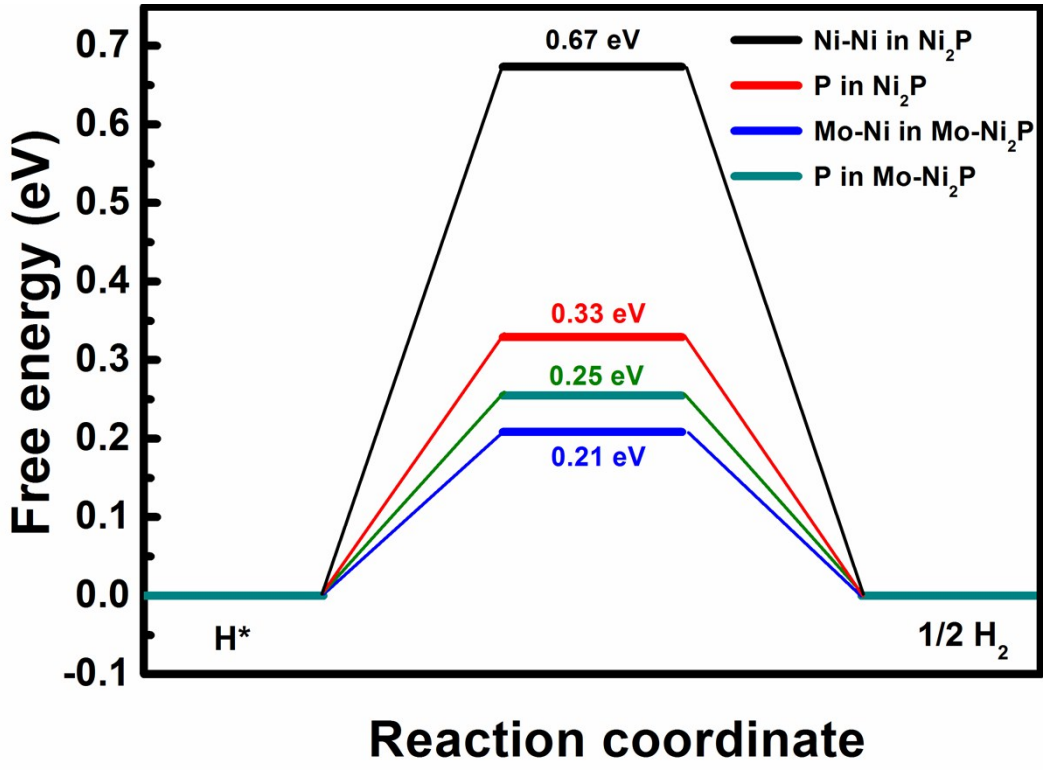

Fig. S14 Free-energy diagram for HER on pristine Ni_2P (111) and Mo-doped Ni_2P (111).

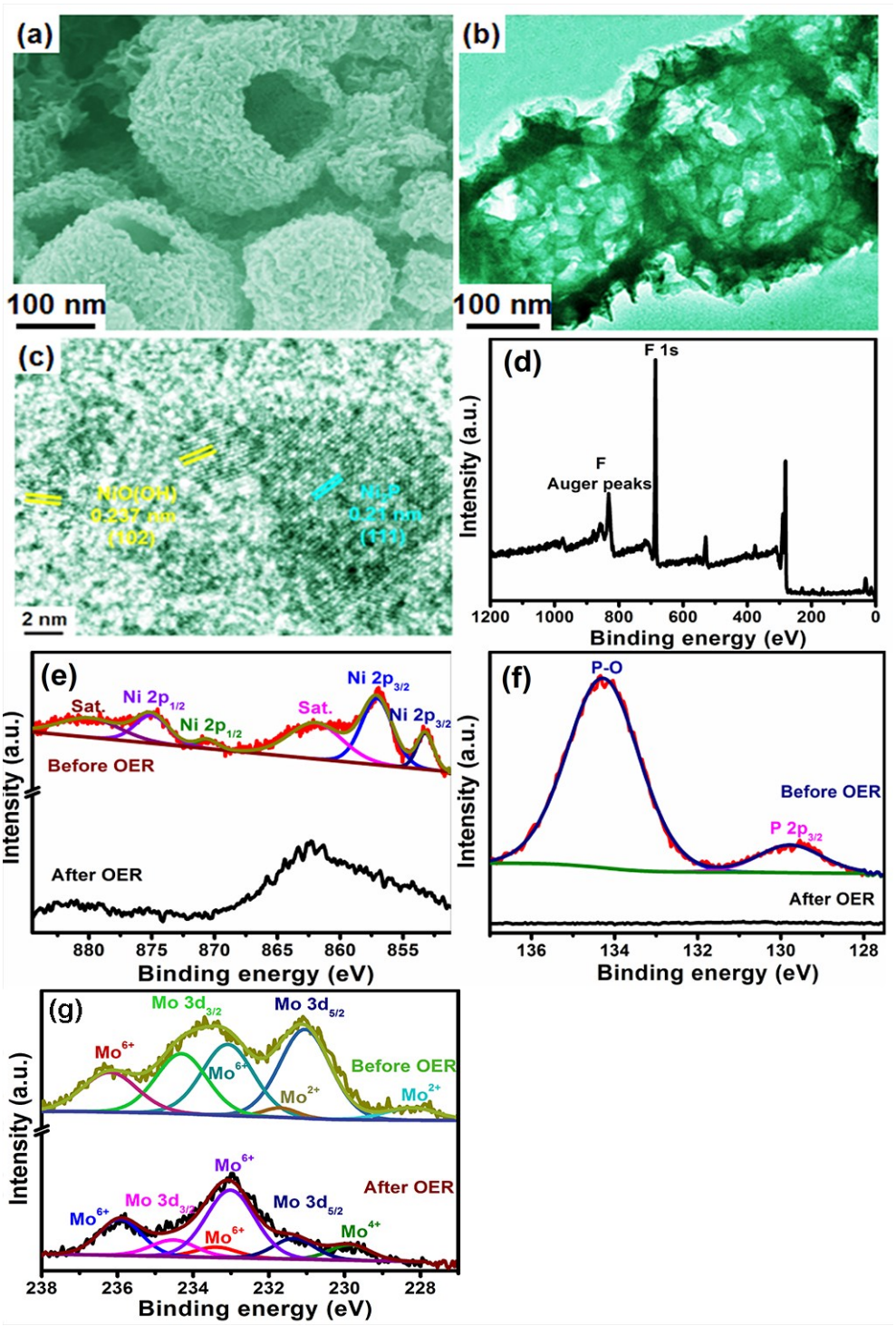

Fig. S15 (a) SEM, (b) TEM and (c) HRTEM images of Mo-doped Ni_2P hollow nanostructures after 10 h OER stability test. Survey scan (d) and high-resolution XPS spectra of the Mo-doped Ni_2P hollow nanostructures after 10h OER stability test: (e) Ni 2p, (f) P 2p and (g) Mo 3d.

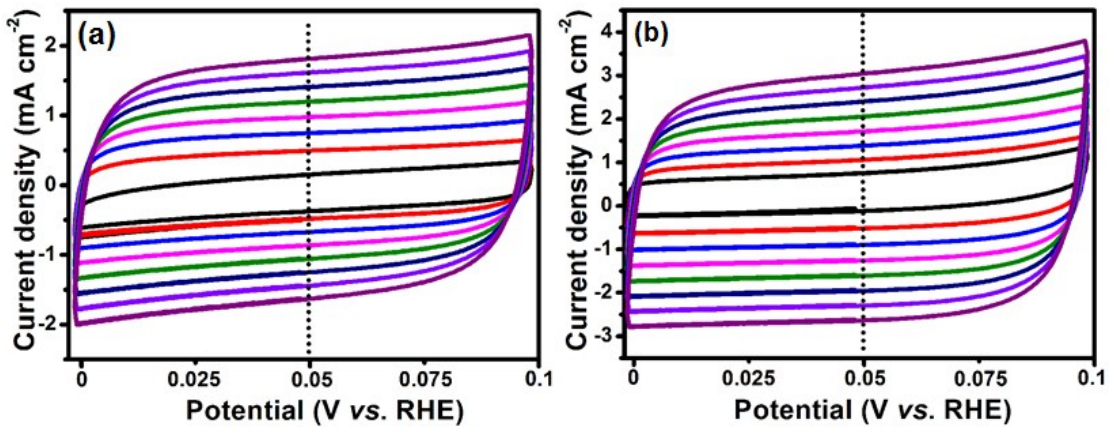

Fig. S16 Voltammograms of the (a) pristine Ni_2P and (b) Mo-doped Ni_2P hollow nanostructures at various scan rates (20-160 mV s^{-1}) during the OER process in alkaline electrolyte.

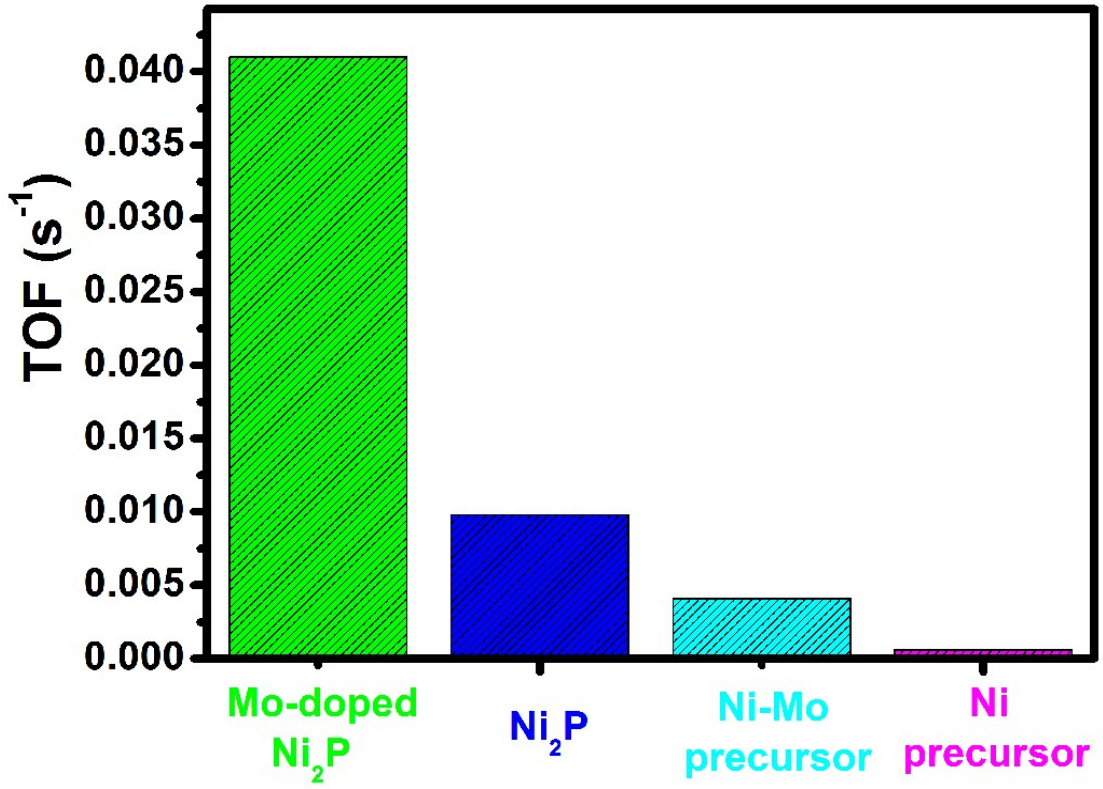

Fig. S17 TOFs of the Mo-doped Ni_2P hollow nanostructure, pristine Ni_2P, Ni-Mo precursor and Ni precursor during the OER process.

Table S1 The detailed additive amount of $(NH_4)_2MoO_4$ for the preparation of Ni-Mo hollow nanostructure electrocatalysts.

	Ni nanoprism precursor (mg)	$(NH_4)_2MoO_4$ (mg)
5.0 % Mo source Ni-Mo hollow nanostructure	57	3
8.3 % Mo source Ni-Mo hollow nanostructure	55	5
11.7 % Mo source Ni-Mo hollow nanostructure	53	7
16.7 % Mo source Ni-Mo hollow nanostructure	50	10

Table S2 Summary of the HER and OER performance using metal-doped transition metal phosphide nanostructures as electrocatalysts.

Catalyst	Overpotential (mV)	Tafel slope (mV dec^{-1})	Electrolyte and loading amount	Reference and current collector
Mo-doped Ni_2P HNs	81 (HER) (10 mA cm^{-2})	53.4 (HER)	1.0 M KOH (0.34 mg cm^{-2})	Our work (glassy carbon)
	270 (OER) (20 mA cm^{-2})	68.5 (OER)	1.0 M KOH	
Mn-doped Ni_2P nanosheet array	103 (HER) (20 mA cm^{-2})	98 (HER)	1.0 M KOH (7.0 mg cm^{-2})	*Chem. Commun.* 2017, **53**, 11048 (Ni foam)
	(OER activity was not reported)			
Mo-doped Ni_2P nanowire array	78 (HER) (10 mA cm^{-2})	82 (HER)	1.0 M KOH (1.13 mg cm^{-2})	*Nanoscale* 2017, **9**, 16674 (Ni foam)
	(OER activity was not reported)			
Mn-doped CoP nanosheet array	76 (HER) (10 mA cm^{-2})	52 (HER)	1.0 M KOH (5.61 mg cm^{-2})	*ACS Catal.* 2017, **7**, 98 (Ti mesh)
	(OER activity was not reported)			
Ni-Fe-P porous nanorods	79 (HER) (10 mA cm^{-2})	101.2 (HER)	1.0 M KOH Not report loading amount	*J. Mater. Chem. A* 2017, **5**, 2496 (Ni foam)
	256 (OER) (10 mA cm^{-2})	72.6 (OER)	1.0 M KOH	
NiCoP nanonest	62 (HER) (10 mA cm^{-2})	68.2 (HER)	1.0 M KOH (2 mg cm^{-2})	*ACS Catal.* 2017, **7**, 4131 (carbon cloth)
	281 (OER) (10 mA cm^{-2})	76.5 (OER)	1.0 M KOH	
Ni-Cu-P film	120 (HER) (10 mA cm^{-2})	69 (HER)	1.0 M KOH (21 mg cm^{-2})	*ACS Appl. Mater. Interfaces* 2018, **10**, 35224 (Ni sheet)
	(OER activity was not reported)			
Fe-Ni-P nanosheets	106 (HER) (10 mA cm^{-2})	89.7 (HER)	1.0 M KOH (5 mg cm^{-2})	*ACS Appl. Mater. Interfaces* 2017, **9**, 26001 (Ni foam)
	270 (OER) (20 mA cm^{-2})	96 (OER)	1.0 M KOH	
CeO_2-modified Ni_2P nanosheet	131 (HER) (10 mA cm^{-2})	87 (HER)	1.0 M KOH (1.58 mg cm^{-2})	*Inorg. Chem.* 2018, **57**, 584 (Ti mesh)
	(OER activity was not reported)			
Ni_2P Hollow microsphere	214 (HER) (10 mA cm^{-2})	125.4 (HER)	1.0 M KOH (0.283 mg cm^{-2})	*Chem. Mater.* 2017, **29**, 8539 (rotation disk electrode)
	359 (OER) (10 mA cm^{-2})	71.7 (OER)	1.0 M KOH	
Fe-doped Ni_2P nanoarray	214 (HER) (50 mA cm^{-2})	No Tafel slope	1.0 M KOH (1.5 mg cm^{-2})	*Adv. Funct. Mater.* 2017, **27**, 1702513 (Ni foam)
	230 (OER) (50 mA cm^{-2})	55.9 (OER)	1.0 M KOH	